Supporting Information

Crystalline red phosphorus for selectively photocatalytic reduction of CO_2 into CO

Zhuofeng Hu [a,] Yinglong Lu [a], Minghao Liu [a], Xiaoyue Zhang [a] and Junjie Cai [b,]**

[a]School of Environmental Science and Engineering, Guangdong Provincial Key Laboratory of Environmental Pollution Control and Remediation Technology, Sun Yat-sen University, Guangzhou 510275, China

[b]School of Materials and Energy, Guangdong University of Technology, Guangzhou 510006, China

Keywords: Red Phosphorus, CO_2 reduction, charge transfer, solar energy.

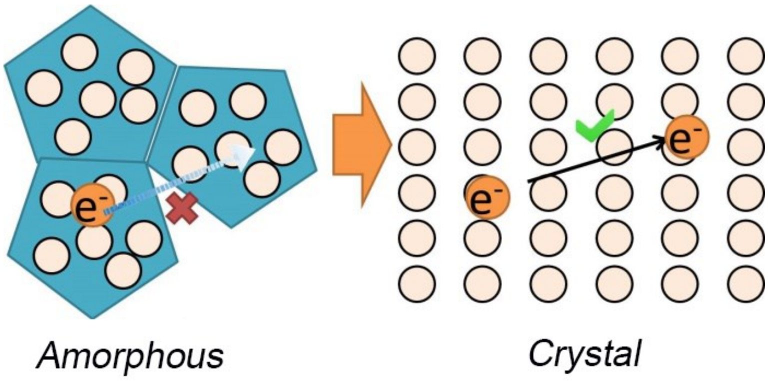

Scheme S1. Diagram comparing the charge transfer in amorphous and crystal structure.

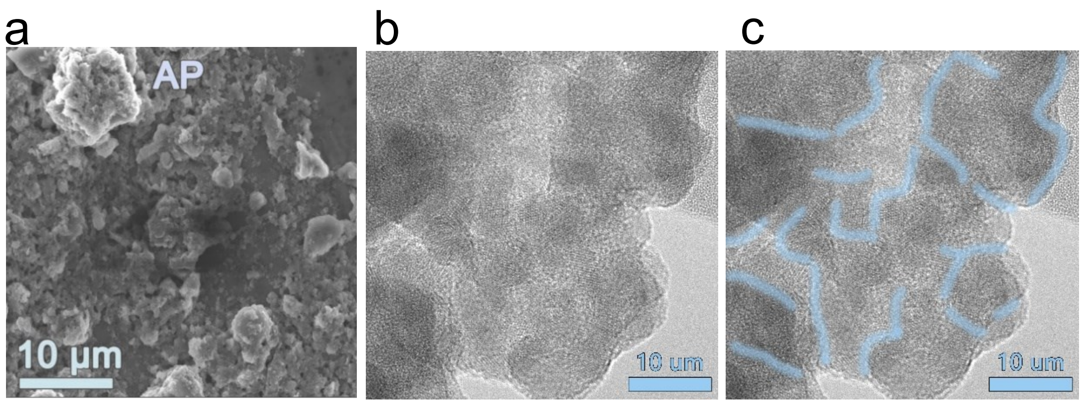

Figure S1. (a) SEM image of amorphous phosphorus; (b) original TEM image of amorphous phosphorus; (c) TEM image highlighting (light blue) the grain interface in amorphous phosphurus

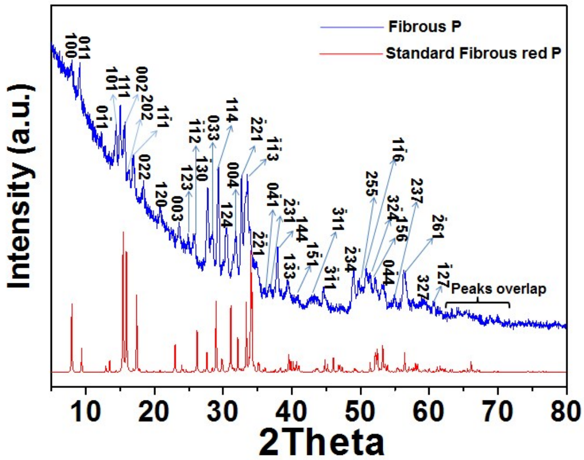

Figure S2. XRD pattern of fibrous red P in detail.

Table S1. The summary of XRD peaks of Fibrous P and standard fibrous red P (CSD391323. cif),

Number	Peaks position (2Theta) (Fibrous red P)	Peaks position (2Theta) (standard fibrous red P)	h	k	l
1	8.00	7.937	1	0	0
2	9.10	9.382	-1	1	0
3	12.62	12.939	1	1	0
4	14.44	14.182	-1	0	1
5	15.10	15.243	0	0	1
6	15.90	15.912	2	0	0
7	16.15	16.099	0	2	0
8	17.13	17.241	-2	0	1
9	18.54	18.827	-2	2	0
10	20.84	20.883	0	-3	1
11	23.64	23.965	3	0	0
12	24.70	24.436	-3	1	1
13	25.90	26.111	2	0	1
14	27.70	27.758	0	-4	1
15	28.40	28.588	-2	0	2
16	29.35	29.695	-4	0	1
17	30.80	30.764	0	0	2
18	31.90	32.141	4	0	0
19	32.60	32.622	1	-4	2
20	33.42	33.304	3	0	1
21	34.04	34.003	-3	4	0
22	35.10	34.889	-4	0	2
23	35.97	35.951	1	4	0
24	36.71	37.013	1	-5	2
25	37.88	38.188	-4	4	0

26	39.56	39.587	4	-4	1
27	40.84	40.762	0	-4	3
28	43.45	43.194	1	-4	3
29	44.65	44.837	-3	3	2
30	49.07	49.160	5	0	1
31	49.80	49.589	0	-7	2
32	50.50	50.410	1	-7	1
33	51.20	50.879	1	0	3
34	52.08	51.976	-6	4	1
35	53.38	53.232	6	-4	1
36	54.80	54.765	4	-7	1
37	56.40	56.660	1	-8	2
38	59.36	59.133	-2	0	4
39	60.70	60.902	1	4	2

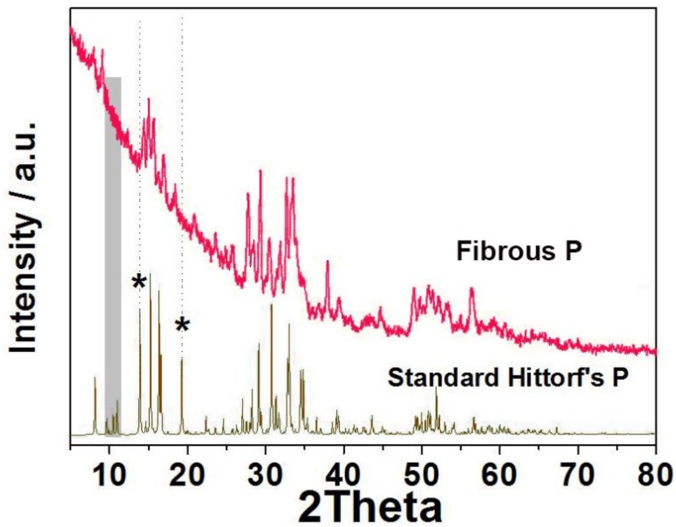

Figure S3. Comparison of the XRD pattern for experimental-synthesized fibrous P and standard hittorf's P

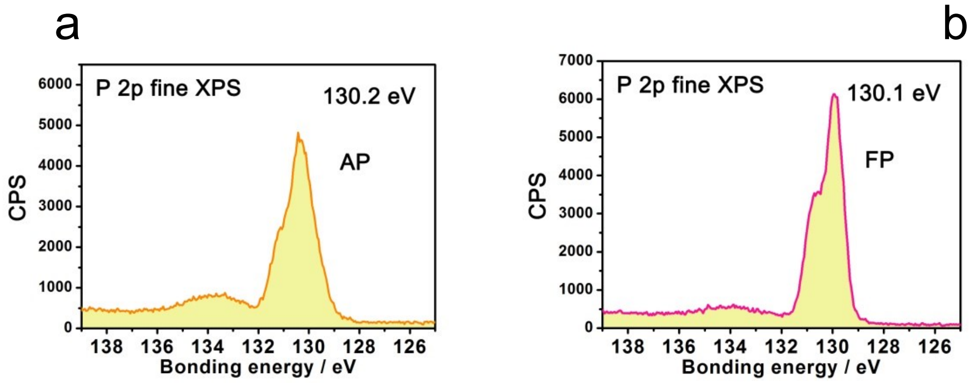

Figure S4. The P 2p fine XPS spectra of (a) amorphous P and (b) fibrous P

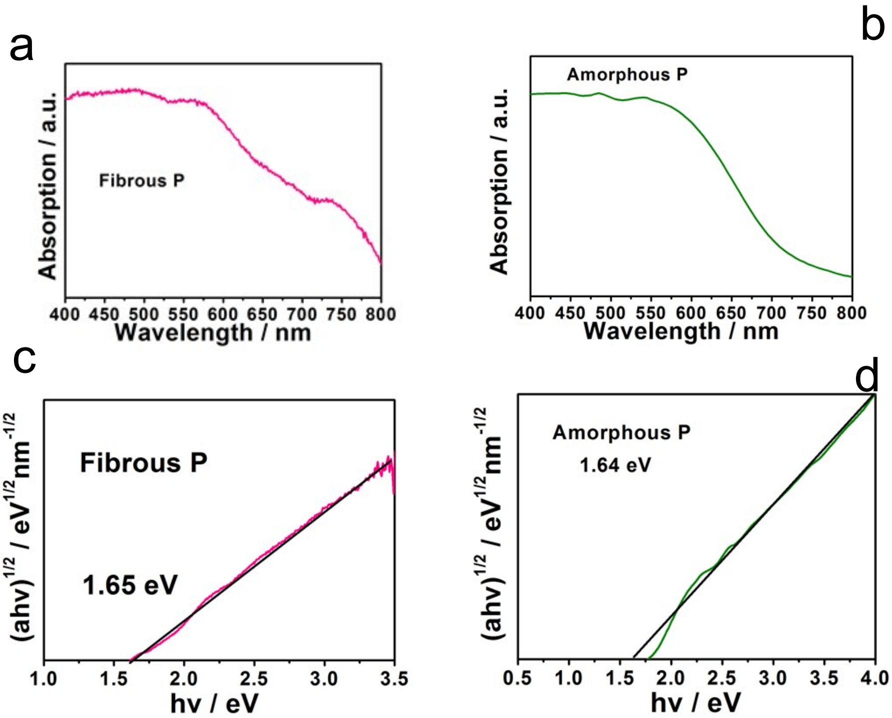

Figure S5. Absorption spectra of (a) fibrous P and (b) amorphous P. Kubelka–Munk plots converted from the absorption spectra of (a) fibrous P and (b) amorphous P.

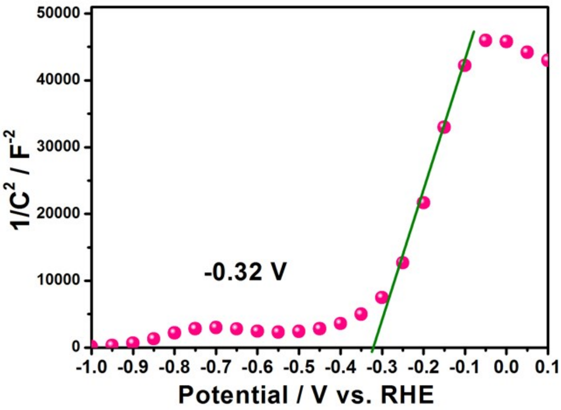

Figure S6. Mott-Schottky plot of fibrous P

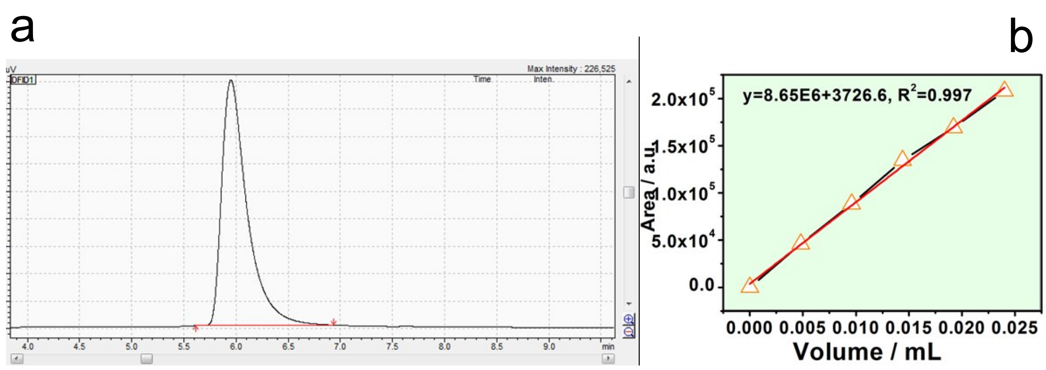

Figure S7. GC curve showing the formation of CO and (b) standard curve showing the peak area as a function of CO volume.

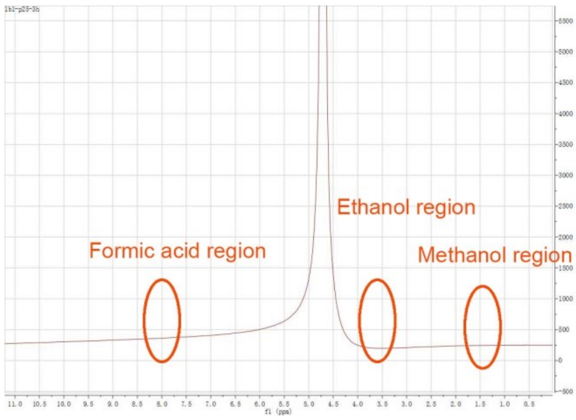

Figure S8. Hydrogen nuclear magnetic resonance spectrum of solution after CO_2 reduction on fibrous P. No peak related to formic acid, methanol or ethanol can be found.

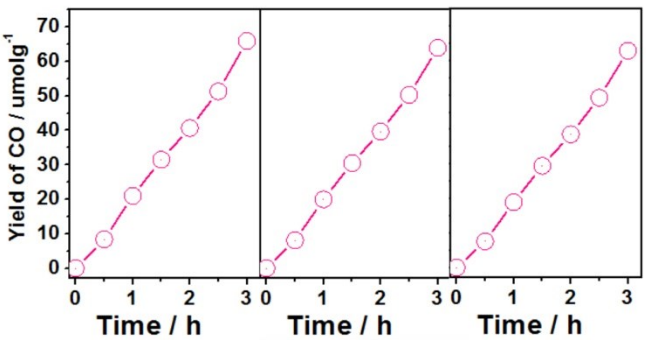

Figure S9. Cycling test of CO_2 reduction into CO on Fibrous P.

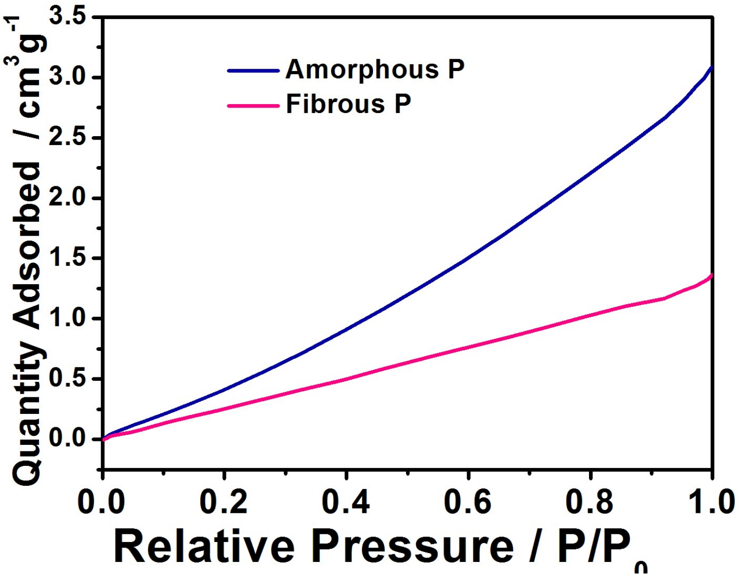

Figure S10. CO_2 adsorption curve of amorphous P and fibrous P

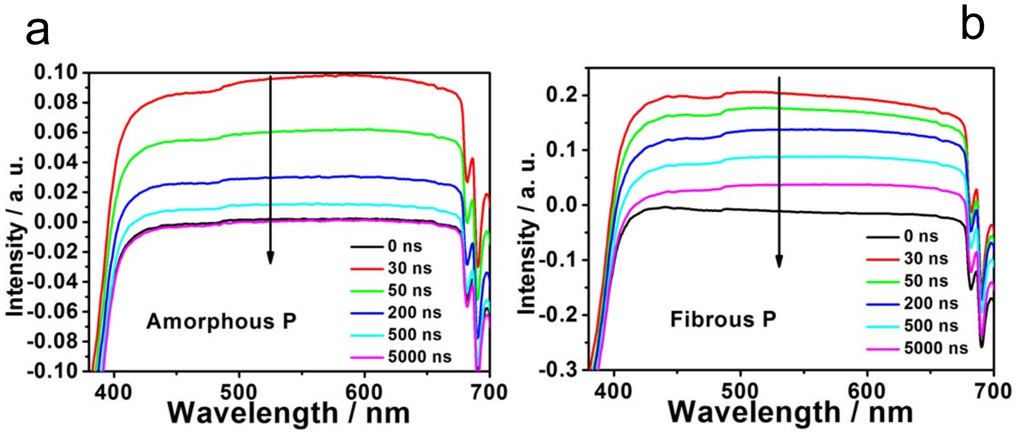

Figure S11. Nanosecond of transient absorption spectra of (a) amorphous and (b) crystalline red phosphorus.

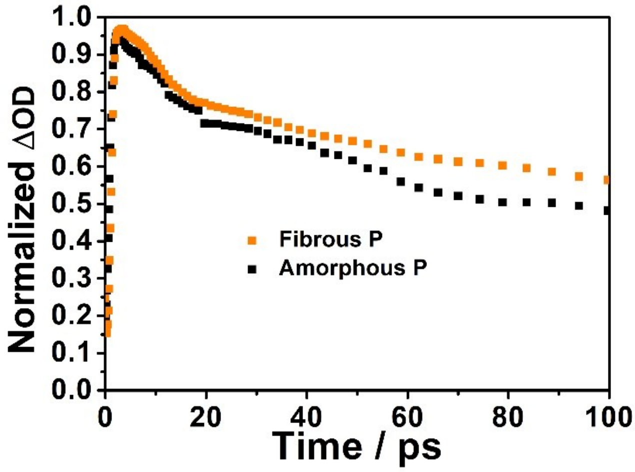

Figure S12. Magnified femtosecond absorption transient spectrum of amorphous P and fibrous P in the beginning 100 ps.

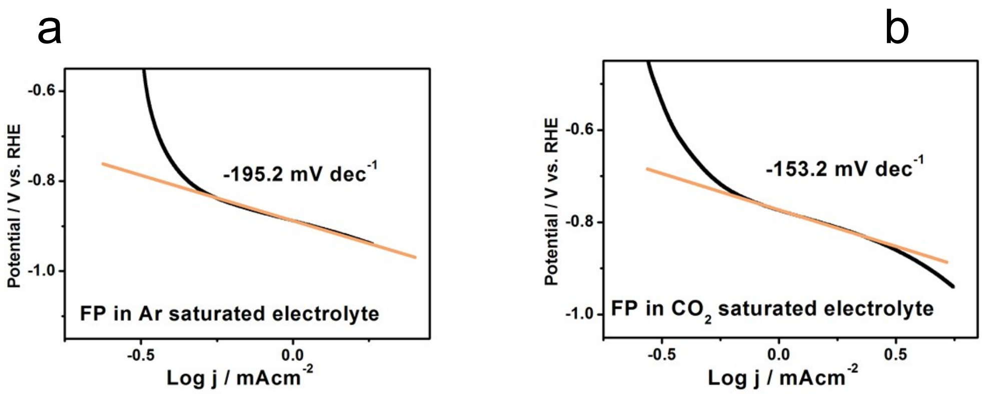

Figure S13. Tafel plot of fibrous P in (a) Ar, and (b) CO_2 saturated 1M $KHCO_3$ electrolyte

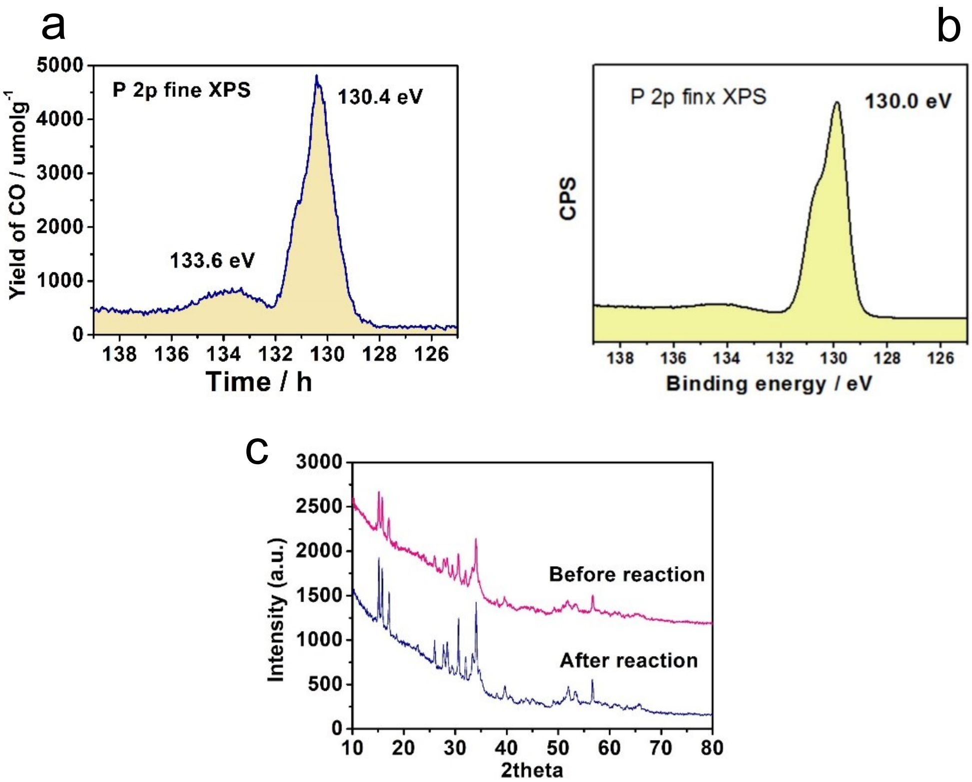

Figure S14. Fine XPS spectrum of P 2p for fibrous P (a) before and (b) after photocatalytic reaction without Ar sputtering. (c) XPS spectrum of P 2p for fibrous P after photocatalytic reaction with 300 s Ar sputtering. (d) XRD pattern of Fibrous P before and after photocatalytic CO_2 reduction.

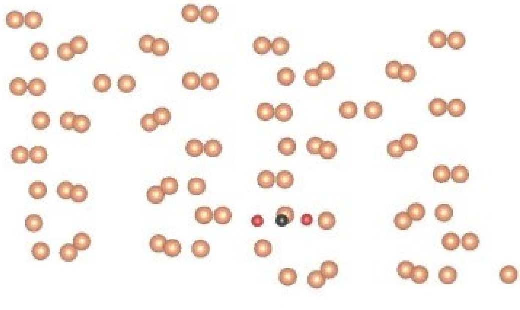

Figure S15. Top view of CO_2-FP system after structure relaxation.

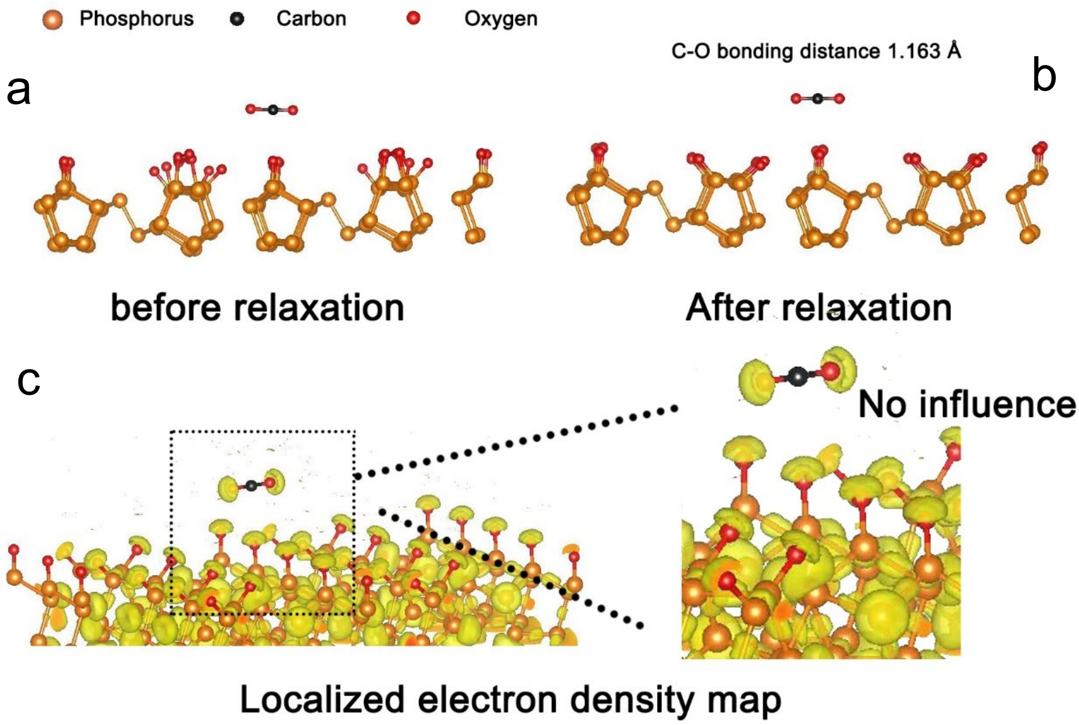

Figure S16. Structure of fibrous P with an oxygen layer (a) before, and (b) after structure relxation. (c) Localized electron density map.

It is clearly that the CO_2 does not infuence the localized electron density of the substrate when the phosphorus surface is cover with oxygen, which is different from the pure phosphorus substrate.

Table S2. Summary of recent-published (2018-2020) report of photocatalytic CO_2 reduction to CO. In the Reaction condition, gas system means the reaction is carried out by putting photocatalyst particles in CO_2 gas atmosphere, while liquid means the photocatalyst particles are dispersed in CO_2 bubbled solution.

No.	Materials	Generation rate of CO (μmol h^{-1} g^{-1})	Reaction condition	Ref.
1	Ti_3C_2 MXene/g-C_3N_4 nanosheets	5.19	gas system; visible light irradiation ($\lambda \geq 420$ nm); 300W Xenon lamp (PLS-SXE300) with a 420 nm cut-off filter	1
2	g-C_3N_4	3.3	liquid system; H_2 production:300W xenon lamp (equipped with a 420 nm cutoff filter; CO_2 Reduction:300 W Xe lamp with an AM1.5 filter	2
3	hierarchical flower-like g-C_3N_4	18.8	gas system; 300W Xe lamp irradiation	3
4	Ternary g-C_3N_4/ZnNCN@ZIF-8	0.45	gas system; 300W full spectrum xenon lamp	4
5	Amino-Assisted NH_2-UiO-66 Anchored on Porous g-C_3N_4	31	liquid system; 300W Xe arc lamp equipped with a 400 nm cutoff filter	5
6	3%Ni/NiO/C_3N_4	27	liquid system; xenon lamp irradiation	6
7	2%Cu/S/C_3N_4	2.4	liquid system; 500W Xe arc lamp (filters light below 335 nm,under visible-light irradiation)	7
8	g-C_3N_4@CeO_2	16.8	liquid system; 300W Xe light with a 420 nm cutoff filter	8
9	Z-Scheme g-C_3N_4/$FeWO_4$	6.2	liquid system; 300W xenon lamp	9
10	NiO/g-C_3N_4	4.17	liquid system; 300 W Xenon-arc lamp	10

11	Au@g-C_3N_4/SnS	17.1	liquid system; 300W Xe light with a 420 nm cutoff filter	11
12	$CsPbBr_3$ QDs /C_3N_4	149	liquid system; 300W Xe-lamp equipped with a 420 nm cut-off filter	12
13	Mg/g-C_3N_4	4.13	liquid system; 300W Xenon-arc lamp	13
14	Fe_2O_3/g-C_3N_4	27	gas system; xenon lamp with a focus intensity of 0.21 W cm^{-2}	14
15	ZnO Micro/nanomaterials	3.81	gas system; under sunlight irradiation	15
16	Cu/TiO_2 catalysts	60	gas system; A Xe arc source system (Newport, Model 63220) was the irradiation source and a liquid cooler was mounted to absorb the infrared portion of the light.	16
17	N-doped TiO_2	0.11	gas system; a Xe lamp (equipped with a cut off filter for infrared for wavelengths above 600 nm)	17
18	Au-25@ZIF-8@TiO_2	132	liquid system; 300 W Xe lamp (420 nm cut-off filter	18
19	vertically aligned rutile TiO_2 (r-TiO_2) nanorod	0.138	liquid system; 300W Xenon arc lamp	19
20	Cu Ultrathin TiO_2 Nanosheet	1.9	liquid system; 300W Xe arc lamp	20
21	Eu-doped TiO_2	42.9	liquid system; 300W Xenon-arc lamp	21
22	Au-TiO_2	2.0	gas system; 200W Hg/Xe lamp with IR filter	22
23	Pd nanoparticle/TiO_2	11.1	gas system; A mercury lamp (500W, >254 nm)	23
24	Mesoporous TiO_2/ 3D Graphene/Layered MoS_2	92.3	liquid system; 300 W Xe lamp	24
25	Hierarchical TiO_2/ Ni(OH)($_2$)	0.76	liquid system; 350 W xenon arc lamp	25
26	cobalt complex/TiO_2	16.8	liquid system; Five non-focused 6W UV lights (Hitachi F6T5, 365 nm)	26
27	BP/C_3N_4	6.54	gas system; 300W Xenon-arc lamp	27

28	$BiVO_4/Bi_4Ti_3O_{12}$	12.39	liquid system; 300W Xe lamp with a focus intensity of 0.2 W cm^{-2}	28
29	Zinc Phthalocyanine/$BiVO_4$	1.0	liquid system; 300 W Xenon arc lamp with a 420 nm cut-off filter	29
30	Black P nanosheets	6.0	liquid system; 200 W Xenon arc lamp, 200 $mWcm^{-2}$	30
31	Black P/ CsPbBr3 composite	44.7	liquid system; 200 W Xenon arc lamp, 200 $mWcm^{-2}$	30
32	Black P	1.5	containing 30 mL of liquid system; with acetonitrile, 10 mL of triethanolamine (TEOA), 300 W Xenon arc lamp	31
33	Black P/ Covalent Triazine Framework	4.6	liquid system; with acetonitrile, 10 mL of triethanolamine (TEOA), 300 W Xenon arc lamp	31
34	Amorphous red P	2.1	gas system 300 W Xenon arc lamp with a 420 nm cut-off filter	This work
35	Fibrous red P	22	gas system 300 W Xenon arc lamp with a 420 nm cut-off filter	This work

Reference

(1) Yang, C.; Tan, Q. Y.; Li, Q.; Zhou, J.; Fan, J. J.; Li, B.; Sun, J.; Lv, K. L., 2D/2D Ti3C2 MXene/g-C3N4 nanosheets heterojunction for high efficient CO2 reduction photocatalyst: Dual effects of urea. *Appl Catal B-Environ* **2020**, 268, 11.

(2) Yuan, J.; Yi, X.; Tang, Y.; Liu, C.; Luo, S., Efficient Photocatalytic Hydrogen Evolution and CO2 Reduction: Enhanced Light Absorption, Charge Separation, and Hydrophilicity by Tailoring Terminal and Linker Units in g-C3N4. *ACS applied materials & interfaces* **2020**, 12, 19607-19615.

(3) Li, F.; Zhang, D.; Xiang, Q., Nanosheet-assembled hierarchical flower-like g-C3N4 for enhanced photocatalytic CO2 reduction activity. *Chem. Commun.* **2020**, 56, 2443-2446.

(4) Xie, Y.; Zhuo, Y. F.; Liu, S. W.; Lin, Y. N.; Zuo, D. R.; Wu, X.; Li, C. H.; Wong, P. K., Ternary g-C3N4/ZnNCN@ZIF-8 Hybrid Photocatalysts with Robust Interfacial Interactions and Enhanced CO2 Reduction Performance. *Sol. RRL*, 12.

(5) Wang, Y. N.; Guo, L. N.; Zeng, Y. Q.; Guo, H. W.; Wan, S. P.; Ou, M.; Zhang, S. L.; Zhong, Q., Amino-Assisted NH2-UiO-66 Anchored on Porous g-C3N4 for Enhanced Visible-Light-Driven CO2 Reduction. *Acs Applied Materials & Interfaces* **2019**, 11, 30673-30681.

(6) Han, C. Q.; Zhang, R. M.; Ye, Y. H.; Wang, L.; Ma, Z. Y.; Su, F. Y.; Xie, H. Q.; Zhou, Y.; Wong, P. K.; Ye, L. Q., Chainmail co-catalyst of NiO shell-encapsulated Ni for improving photocatalytic CO2 reduction over g-C3N4. *J Mater Chem A* **2019**, 7, 9726-9735.

(7) Ojha, N.; Bajpai, A.; Kumar, S., Visible light-driven enhanced CO2 reduction by water over Cu modified S-doped g-C3N4. *Catal Sci Technol* **2019**, 9, 4598-4613.

(8) Liang, M. F.; Borjigin, T.; Zhang, Y. H.; Liu, B. H.; Liu, H.; Guo, H., Controlled assemble of hollow heterostructured g-C3N4@CeO2 with rich oxygen vacancies for enhanced photocatalytic CO2 reduction. *Appl Catal B-Environ* **2019**, 243, 566-575.

(9) Bhosale, R.; Jain, S.; Vinod, C. P.; Kumar, S.; Ogale, S., Direct Z-Scheme g-C3N4/FeWO4 Nanocomposite for Enhanced and Selective Photocatalytic CO2 Reduction under Visible Light. *Acs Applied Materials & Interfaces* **2019**, 11, 6174-6183.

(10) Tang, J. Y.; Guo, R. T.; Zhou, W. G.; Huang, C. Y.; Pan, W. G., Ball-flower like NiO/g-C3N4 heterojunction for efficient visible light photocatalytic CO2 reduction. *Appl Catal B-Environ* **2018**, 237, 802-810.

(11) Liang, M. F.; Borjigin, T.; Zhang, Y. H.; Liu, H.; Liu, B. H.; Guo, H., Z-Scheme Au@Void@g-C3N4/SnS Yolk-Shell Heterostructures for Superior Photocatalytic CO2 Reduction under Visible Light. *Acs Applied Materials & Interfaces* **2018**, 10, 34123-34131.

(12) Ou, M.; Tu, W. G.; Yin, S. M.; Xing, W. N.; Wu, S. Y.; Wang, H. J.; Wan, S. P.; Zhong, Q.; Xu, R., Amino-Assisted Anchoring of CsPbBr3 Perovskite Quantum Dots on Porous g-C3N4 for Enhanced Photocatalytic CO2 Reduction. *Angew Chem Int Edit* **2018**, 57, 13570-13574.

(13) Tang, J. Y.; Zhou, W. G.; Guo, R. T.; Huang, C. Y.; Pan, W. G., Enhancement of photocatalytic performance in CO2 reduction over Mg/g-C3N4 catalysts under visible light irradiation. *Catalysis Communications* **2018**, 107, 92-95.

(14) Jiang, Z. F.; Wan, W. M.; Li, H. M.; Yuan, S. Q.; Zhao, H. J.; Wong, P. K., A Hierarchical Z-Scheme alpha-Fe2O3/g-C3N4 Hybrid for Enhanced Photocatalytic CO2 Reduction. *Adv Mater* **2018**, 30, 9.

(15) Liu, X. D.; Ye, L. Q.; Liu, S. S.; Li, Y. P.; Ji, X. X., Photocatalytic Reduction of CO2 by ZnO Micro/nanomaterials with Different Morphologies and Ratios of {0001} Facets. *Scientific Reports* **2016**, 6, 9.

(16) Li, Y.; Wang, W. N.; Zhan, Z. L.; Woo, M. H.; Wu, C. Y.; Biswas, P., Photocatalytic reduction of CO2 with H2O on mesoporous silica supported Cu/TiO2 catalysts. *Appl Catal B-Environ* **2010**, 100, 386-392.

(17) Bjelajac, A.; Kopac, D.; Fecant, A.; Tavernier, E.; Petrovic, R.; Likozar, B.; Janackovic, D., Micro-kinetic modelling of photocatalytic CO2 reduction over undoped and N-doped TiO2. *Catal Sci Technol* **2020**, 10, 1688-1698.

(18) Tian, L. Y.; Luo, Y. C.; Chu, K. L.; Wu, D. J.; Shi, J. Y.; Liang, Z. X., A robust photocatalyst of Au-25@ZIF-8@TiO2-ReP with dual photoreductive sites to promote photoelectron utilization in H2O splitting to H-2 and CO2 reduction to CO. *Chem. Commun.* **2019**, 55, 12976-12979.

(19) Sun, R. K.; Jiang, X. L.; Zhang, M. L.; Ma, Y. Y.; Jiang, X.; Liu, Z. Q.; Wang, Y. Q.; Yang, J. L.; Xie, M. Z.; Han, W. H., Dual quantum dots decorated TiO2 nanorod arrays for efficient CO2 reduction. *Journal*

Of Catalysis **2019**, 378, 192-200.
(20) Jiang, Z. Y.; Sun, W.; Miao, W. K.; Yuan, Z. M.; Yang, G. H.; Kong, F. G.; Yan, T. J.; Chen, J. C.; Huang, B. B.; An, C. H.; Ozin, G. A., Living Atomically Dispersed Cu Ultrathin TiO2 Nanosheet CO2 Reduction Photocatalyst. *Advanced Science* **2019**, 6, 5.
(21) Chun-ying, H.; Rui-tang, G.; Wei-guo, P.; Jun-ying, T.; Wei-guo, Z.; Hao, Q.; Xing-yu, L.; Peng-yao, J., Eu-doped TiO2 nanoparticles with enhanced activity for CO2 photocatalytic reduction. *Journal of CO2 Utilization* **2018**, 26, 487-495.
(22) Pougin, A.; Dodekatos, G.; Dilla, M.; Tuysuz, H.; Strunk, J., Au@TiO2 Core-Shell Composites for the Photocatalytic Reduction of CO2. *Chemistry-a European Journal* **2018**, 24, 12416-12425.
(23) Xu, C. Y.; Huang, W. H.; Li, Z.; Deng, B. W.; Zhang, Y. W.; Ni, M. J.; Cen, K. F., Photothermal Coupling Factor Achieving CO2 Reduction Based on Palladium-Nanoparticle-Loaded TiO2. *Acs Catalysis* **2018**, 8, 6582-6593.
(24) Jung, H.; Cho, K. M.; Kim, K. H.; Yoo, H. W.; Al-Saggaf, A.; Gereige, I.; Jung, H. T., Highly Efficient and Stable CO2 Reduction Photocatalyst with a Hierarchical Structure of Mesoporous TiO2 on 3D Graphene with Few-Layered MoS2. *ACS Sustain. Chem. Eng.* **2018**, 6, 5718-5724.
(25) Meng, A. Y.; Wu, S.; Cheng, B.; Yu, J. G.; Xu, J. S., Hierarchical TiO2/Ni(OH)(2) composite fibers with enhanced photocatalytic CO2 reduction performance. *J Mater Chem A* **2018**, 6, 4729-4736.
(26) Lin, J. L.; Sun, X. X.; Qin, B.; Yu, T., Improving the photocatalytic reduction of CO2 to CO for TiO2 hollow spheres through hybridization with a cobalt complex. *Rsc Advances* **2018**, 8, 20543-20548.
(27) Han, C. Q.; Li, J.; Ma, Z. Y.; Xie, H. Q.; Waterhouse, G. I. N.; Ye, L. Q.; Zhang, T. R., Black phosphorus quantum dot/g-C3N4 composites for enhanced CO2 photoreduction to CO. *Science China-Materials* **2018**, 61, 1159-1166.
(28) Wang, X. Y.; Wang, Y. S.; Gao, M. C.; Shen, J. N.; Pu, X. P.; Zhang, Z. Z.; Lin, H. X.; Wang, X. X., BiVO4/Bi4Ti3O12 heterojunction enabling efficient photocatalytic reduction of CO2 with H2O to CH3OH and CO. *Appl Catal B-Environ* **2020**, 270, 9.
(29) Bian, J.; Feng, J. N.; Zhang, Z. Q.; Li, Z. J.; Zhang, Y. H.; Liu, Y. D.; Ali, S.; Qu, Y.; Bai, L. L.; Xie, J. J.; Tang, D. Y.; Li, X.; Bai, F. Q.; Tang, J. W.; Jing, L. Q., Dimension-Matched Zinc Phthalocyanine/BiVO4 Ultrathin Nanocomposites for CO2 Reduction as Efficient Wide-Visible-Light-Driven Photocatalysts via a Cascade Charge Transfer. *Angew Chem Int Edit* **2019**, 58, 10873-10878.
(30) Wang, X.; He, J.; Li, J.; Lu, G.; Dong, F.; Majima, T.; Zhu, M., Immobilizing perovskite CsPbBr3 nanocrystals on Black phosphorus nanosheets for boosting charge separation and photocatalytic CO2 reduction. *Applied Catalysis B: Environmental* **2020**, 277, 119230.
(31) Li, J.; Liu, P.; Huang, H. L.; Li, Y.; Tang, Y. Z.; Mei, D. H.; Zhong, C. L., Metal-Free 2D/2D Black Phosphorus and Covalent Triazine Framework Heterostructure for CO2 Photoreduction. *ACS Sustain. Chem. Eng.* **2020**, 8, 5175-5183.